Empirical Assessment of Ultrasound Model Based Reconstructive Elasticity Imaging

Mashsa Abassi

University of Maryland Medical Center, 655 W. Baltimore Street, Baltimore MD 21201.

mashsaabassii@hotmail.com

Correspondence should be addressed to **Mashsa Abassi** : mashsaabassii@hotmail.com

Abstract – In order to rebuild the spatial distribution of Young's modulus, Elasticity Imaging (EI) employs state-of-the-art imaging technology to quantify the displacement of tissues in response to mechanical stimulation. In this paper, we provide a method for ultrasonic EI that makes use of the Model-Based Reconstruction (MBR) approach to Young's modulus reconstruction. Since the object being imaged has an unusual shape, only the longitudinal element of the strain matrix is employed. The technique is particularly successful in its numerical implementation since it uses an analytic solution to the Elasticity Reconstruction (ER) problem. The categorization of liver hemangiomas and the staging of Deep Venous Thrombosis (DVT) are two potential clinical applications of the model-based approach. In sum, these researches show that model-based prosthetic EI may be useful provided both the item's shape and its neighboring cells are understood, and when specific assertions about the pathologies could be established.

Keywords – Elasticity Imaging (EI), Elasticity Reconstruction (ER), Model-Based Reconstruction (MBR), Deep Venous Thrombi.

I. INTRODUCTION

Techniques for Ultrasound Elasticity Imaging (USEI) [1], such as Supersonic Shear Imaging (SSI) [2], Shear Wave Elasticity Imaging (SWEI) [3], Spatially Modulated Ultrasound Radiation Force (SMURF) [4] imaging, Comb-Push Ultrasound Shear Elastography (CUSE) [5], and Acoustic Radiation Force Impulse (ARFI) [6] imaging, have been described in recent years. Conventional ultrasound imaging techniques are utilized to monitor the movements of tissues that have been induced by the focussed ultrasound beams' acoustic radiation force. ARFI imaging employs on-axis material motion to identify relative variations in elasticity, similar to the data acquired by push imaging procedures. Other methods, on the other hand, measure tissue stiffness by tracking tissue motion at distant places from the ARFI activation in order to determine the speed of dispersion of the associated shear waves.

Tracking the shear wavesout of one ARFI stimulation is traditionally done using numerous track beams in the SWEI technique. The elastic strength between the tracks beams employed in the estimate is reflected in the Shear Wave Speed (SWS) [7] that is produced. The SSI and CUSE techniques both make use of standard tracking setups;however, their push focal adjustments are unique. These techniques are collectively known as MTL-SWEI (Multiple Track Location SWEI), since they use numerous track positions for a single push position. SMURF imaging, on the other hand, makes use of a number of push beams that are laterally offset from one another and a single-trackgrin. Between the push beams, SMURF estimates a SWS that is reflective of the tissue characteristics. This technique is known as STL-SWEI (Single Track Location SWEI). More energy is deposited into the tissue during STL-SWEI SWS measurements because of the need for numerous ARFI excitations.The resulting motion of interior tissues may be measured using ultrasound, Magnetic Resonance Imaging (MRI), or another technique. The dispersion of the strain vector elements is used to assess the modulus (Young's modulus) dispersion using inverse problem frameworks. Although Elasticity Imaging (EI)'s first use was in
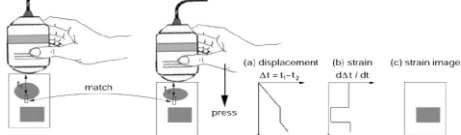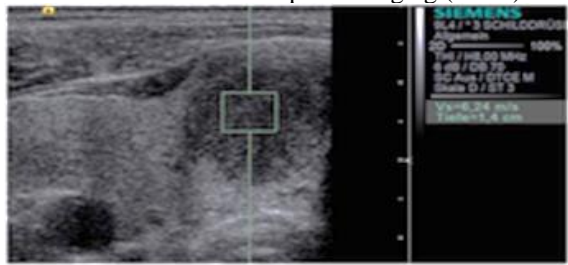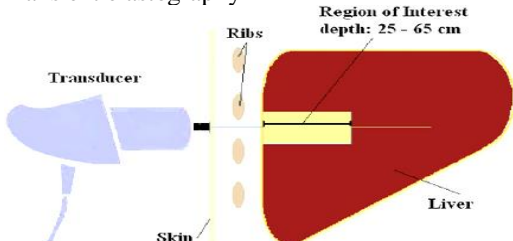
noninvasive cancer diagnosis, it has now been shown to be applicable in a wide range of other fields, such as atherosclerotic plaque identification, corneal cataract surgery, heart strain detection, muscle dynamics, and so on.

The strain imaging in the tissue may be created after the motion of the tissue's interior has been monitored. Contrast in strain pictures is affected by the tissue flexibility because hard tissue areas are often less deformed than soft tissue parts. The strain field, however, is sensitive not only to the elastic distributions but also to the universal boundary layer, which could be rather complicated in biological tissues. Due to the ambiguity between strain imaging and tissue elasticity distributions, quantifiable determination of tissue elasticity needs Young's modulus reconstructions. Many different questions might be asked about recalculating the elastic modulus of an inhomogeneous material from external observations of internal displacements. These methods may be broken down into two broad classes: direct methods and indirect (model-based) methods. If the modeling of the intrinsic distribution orientations and strain vector is supplied at a given point, then the unknown dispersion of Young's or moduli at that place may be characterized using reconstruction approaches based on the static equations. Unfortunately, the inverse issue with an arbitrary geometry as well as elasticity distributions is notoriously difficult to express and solve in direct reconstruction approaches.

Nevertheless, the inverse issue may be addressed by using iterative resolutions of forward problems with tweaked elasticity values, provided that some previous information or assumptions about the shape of the object and model parameters can be established. A Model-Based Reconstruction (MBR) [8]is possible if the object's shape or certain other assumptions allow for the modeling of localized changes in elasticity. Since the presence of the pathology may be inferred from the imaging research, model-based Elasticity Imaging (EI) [9] approaches may be applicable in settings where pathology characterisation rather than detection is needed. In many instances, we have enough information to make educated guesses regarding the distribution of elasticity in the tissues around the disease and its approximate position and shape. It is important to keep in mind that the relative elasticity distribution is the only thing that can be learned by either the direct or model-based techniques. Reconstructing the Young's modulus to an absolute value requires either a point of reference or stress data.

Because ultrasound allows the speckle's mobility to be followed across such a broad range of tissue deformations, it is often utilized in EI. Examples of ultrasonic elastography are included in **Table 1**.
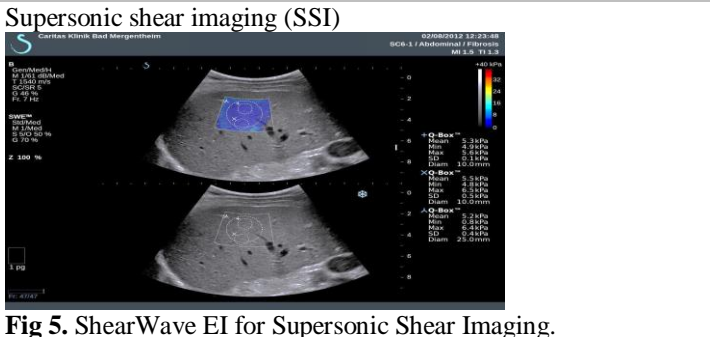
<div align="center">Table 1. Examples of ultrasonic elastography</div>

US Elastography Method and Illustration	Brief Description
Quasistatic elastography / strain imaging **Fig 1.** The basics of strain imaging in quasi-static conditions. The elliptical structure is as rigid as the backdrop, whereas the rectangle framework is more so.	For historical reasons, the term "elastography" is sometimes used interchangeably with "quasistatic elastography," which is one of the early elastography methods. This method involves compressing tissue from the outside and then comparing ultrasonic pictures taken prior to and after the compression.
Acoustic radiation force impulse imaging (ARFI) **Fig 2.** The right thyroid lobe nodule, as shown in an ARFI picture.	To generate a qualitative two-dimensional map of tissue stiffness, ultrasound is used in a methodology known as ARFI (Acoustic Radiation Force Impulse Imaging). This is accomplished by directing a concentrated beam of ultrasonic energy into the tissue, where its acoustic radiation force causes a "push" deep inside.
Transient elastography **Fig 3.** An illustration of a transient elastography device for evaluating liver stiffness.	In terms of picture quality, transient elastography is superior to other methods since it provides a quantitative, single line (i.e., 1-D) representation of tissue elasticity. The motor vibrates the skin, causing a transient deformation in the tissues (shear waves), which is then imaged by a 1D ultrasound wave as it travels further into the body.
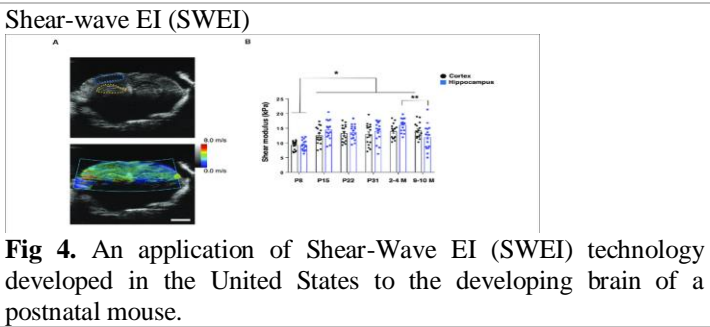
Shear-wave EI (SWEI)	Similar to ARFI, Shear-Wave EI (SWEI) employs conventional ultrasonic force to create a 'push' deeper into the tissues. The pressure-induced disruption propagates as a shear pulse along the tissue's lateral dimensions.
Fig 4. An application of Shear-Wave EI (SWEI) technology developed in the United States to the developing brain of a postnatal mouse.	
Supersonic shear imaging (SSI)	Systematic, authentic, two-dimensional mapping of tissue elasticity is made possible by Supersonic Shear Imaging (SSI).
Fig 5. ShearWave EI for Supersonic Shear Imaging.	

While the axial element of the vector field can be reliably estimated, the lateral component cannot. True, an ultrasound system's lateral precision is dictated by the breadth of the ultrasonic beam, while its axial resolution is principally restricted by the frequency and bandwidth of the transducers. Because all displacement components and relative positions are necessary for direct reconstructions approaches, anisotropy in the accuracy of the wave vector measurement adds to the total noise level in elasticity images. Model-based methods, on the other hand, may be developed using just the axial element of the vector field, guaranteeing that the accuracy of the reconstructed Young's modulus is unrelated to the precision with which the lateral mobility of the object is tracked.

In this article, we provide an ultrasonic EI technique that employs the Model-Based Reconstruction (MBR) approach to Young's modulus reconstruction. Two possible clinical uses of the model-based approach addressed in this study are the classification of hepatic hemangiomas and the staging of Deep Venous Thrombosis (DVT). The remainder of this article is organized as follows: Section II presents a discussion of research objectives and methodology employed to obtain the required results. Section III reviews the previous works in literature concerning EI and the two application cases employed in this paper. In Section IV, critical analysis of results and discussion have been presented, which Section V draws final conclusion to the research.

II. RESEARCH OBJECTIVE AND METHODOLOGY

In this article, we demonstrate the model-based EI technique with cases from two potential clinical applications: the detection of hepatic hemangiomas and the differentiation of Deep Venous Thromboses (DVT). To draw the required results, Liver hemangiomas were thought to be characterized by their spherical symmetry, whereas DVTwas thought to be characterized by their cylindrical form. Both studies used exterior surface deflections during the course of continual ultrasound scans, with tissue mobility measured using a block-matching cross-correlation approach. The Young's modulus was calculated using strain pictures that were measured. These researches prove the viability of model-based prosthetic EI in situations when the object's shape and the neighboring cells can be evaluated and where certain hypotheses about the pathologies can be drawn from ultrasound images

III. LITERATURE REVIEW

Nitta, Shiina, and Ueno [10] provide a novel technique for estimating the elastic modulus of compressed soft tissue. To quantify axial tissue displacement fields, this method uses a correlation methodology on ultrasound waves and the Newton-Raphson method to iteratively adjust a Finite Element (FE) model of the elasticity coefficients to achieve a least-squares fit. Tikhonov regularization is used to fix the Hessian matrix's poor conditioning. The authors propose using the multi-beam method to evaluate the viscoelastic distribution in a three-dimensional tissue structure by measuring the three-dimensional distribution of deformation matrices. The phase difference at each component on the two-dimensional array magnification is exploited by the Weighted Phase Gradient Method (WPGM) [11]. Adding the authors' own "combined stationarity approach" into the WPGM as the phase control detector makes their proposed method applicable to strain metrics for additional weight (i.e., beyond wavelengths). In addition, we make an effort to use the recorded 3-D displacement vectors to recreate the elastic modulus distribution. The viability of our approaches for assessing the 3-D tissue structure was confirmed by numerical simulation.

According to Damascelli et al. [12], up to 70 percent of the population develops hemangioma, making it the most common benign tumor of the liver. Hemangiomas may range from being very small to very enormous, measuring several centimeters in diameter. The tumors themselves are loaded with vascular channels of varying widths and sometimes some fibrous tissue as well. Perhaps the blood vessels are clogged with thrombi, or clots. Hemangiomas have the histologic appearance of enormous, thin-walled vascular system that are completely filled with blood. Ultrasounds and CT scans used for various purposes often reveal these pituitary tumors. There is no need for further therapy once a diagnosis has been made; only big, symptomatic hemangiomas are removed surgically. However, certain imaging procedures, such nuclear medicine imaging with radiological technology-based red blood cell, static CT scans and magnetic resonance with contrasts, are necessary for a diagnosis of hemangioma.

According to Metikala et al. [13], an abnormal growth of blood vessels in the liver is called a hemangioma and is considered benign. Hepatic hemangiomas, sometimes called cavernous hemangiomas, are benign tumors that form in the liver and are found in an estimated 20% of the general population. Liver hemangiomas often present as a hyperechoic area with well-defined borders on an ultrasonography B-Scan picture. But regular ultrasonography is just suggestive and not diagnostic. The B-scan findings of many different liver lesions, including some malignant ones, may be identical. Therefore, it is important to make an accurate diagnosis of a found liver mass in the fastest and cheapest method possible. Hemangiomas are often described as "blood-filled soft lesions" in the medical literature. As a result, EI shows promise as a tool for identifying hemangiomas. Because mechanical features are distributed by most tumor cells and not the background, they may be used to distinguish hypertrophic scars from other liver fibrosis.

According to Adjei et al. [14], the most common preventable cause of mortality among hospitalized patients across the American States and other high-income countries is pulmonary embolism (PE), which occurs as a result of Deep Vein Thrombosis (DVT) [15]. Deep Vein Thrombosis (DVT) occurs when a blood clot forms in a deep vein (often in the leg or knee) and either partially or completely impedes the circulation of blood. in the vein. When a thrombus breaks away from the vascular wall and enters the veins, it might cause pulmonary embolism. Death may occur rapidly from pulmonary embolism if a big clot or embolus becomes lodged in the lung's main blood vessel. An older clot poses a greater threat of a pulmonary embolism and requires more aggressive treatment for deep vein thrombosis (This article often uses the term "blood clot" to allude to deep vein thrombosis). Acute thrombi increase the likelihood of clot fragmentation and subsequent embolus formation. Heparin and then oral anticoagulants are being used to treat this patient. Therapy options for patients with persistent DVT include oral anticoagulants such coumadin, or no treatment at all. One should try to avoid using heparin if at all feasible because to the greater risk of bleeding associated with heparin compared to coumadin. Because of this, differentiating between acute and chronic DVT is crucial in the clinic.

According to Liu et al. [16], thrombus detection may be accomplished through MRI or duplex ultrasonography. While these tools may pinpoint the location of the clot in the vein, they are unable to establish how old it is. Clot elasticity has been shown to be a useful indicator of DVT development. This is predicated on the idea that the ductility of a thrombus varies linearly with the concentrations of fibrin and collagen. The severity of DVT increases with age because thrombus fibrin and collagen levels both rise with time. Therefore, it is possible that remote estimation of thrombus elastic properties might become a valuable clinical tool for predicting the antiquity of a DVT.

IV. RESULTS AND DISCUSSION

ER of Liver Hemangioma

Hemangioma-affected participants were studied to see whether EI could be used to identify and diagnose hemangiomas. The University of Michigan's IRB authorized this research, and all participants provided informed consent. The liver was imaged from directly in front of patient's ribs using a linear 128-component matrix projector and a 5.0 MHz Ultramark 9.0 ATL laser. Over the period of 4 seconds, the program's interconnection with a PCB was used to record 120 panels of electronic Rf communication in real time. When the array was attached to a compressional equipment on a medical trolley (rafter), it pressed against the body, distorting the liver somewhat. As long as the load exerted did not exceed 10-12 mm on the surface, the participants did not report any pain.

Every single experiment used a phase-sensitive correlation-based speckle tracking method to estimate motion from frame to frame. We estimated the 2D distortion from the site of the highest correlation coefficient, and the enhanced axial distortion estimates from the position of the phase 0 convergence of the modulator method correlations. Before estimating displacement, filtering geographically neighboring correlation functions helped minimize displacement error even more. Many additional participants yielded the same findings. Given the tumor's soft core, the strain image's inference of a hemangioma's overall hardness is surprising. However, this finding is in line with data acquired from surgical procedures, where intact hemangiomas are felt as hard lesions when big, symptomatic hemangiomata are removed. However, when pressure is given to the hemangioma, it shatters and bleeds out. Since blood has zero or very little shear elasticity, a hemangioma will feel as hard as a rock even if it is full of blood.

Generally, if a soft, fluid-filled bag is covered by an extremely solid, thin layer, it may appear rigid. To minimize its impact on the stress distribution within the haematoma, a shell must have the same physical behavior as the lesion itself. The tension within the hematoma, nevertheless, is reduced if indeed the shell is harder than the hematoma. Whatever the nature of the interior material, the stress inside the lesion will vanish if the shell is infinitely hard and entirely unresponsive. Because of this, it is reasonable to assume that the light membrane surrounding a hemangioma is much more

robust than the lesion's center, and thus controls the distribution of stress within the tumour cells. Strain distributions are sensitive to the shell's mechanical parameters around a lesion. When it comes to strain imaging, for example, it seems that a homogeneity hard inclusion and a heterogeneity inclusion encircled by a protective shell are both treated the same. In any scenario, however, reconstructive EI may provide a means of approximating the lesion's constituent parts.

Two methods, direct reconstructions and MBR, were used to map Young's modulus for hemangiomaEI [17]. With direct reconstructions, the discretized equilibrium coefficients for a planar strain condition are solved numerically. When conformational changes are applied to the liver through the rib cage, resulting in low out-of-plane pressures, the planar strain situation is a close estimate for determining the extent of the injury. There is no need for previous information about the item, and no additional assumptions are required, while using this technique. The distribution of Young's modulus is rebuilt with respect to the modulus of the surrounding tissue once an area of interest including the lesion has been defined (i.e., liver).Assuming the hemangioma can be represented by a sphere, we could utilize a model-based approach in which the deformation within the scanning plane is typically a measurement of radial position from the tumor's axis. It's a decent stand-in for a real tumor if you remove all the surrounding tissue. When compared to compared to the conventional ERs, the MBR near the cancer cell core is much more resistant to strain noise when a simple model is assumed.

The calculated elasticity values are shown in **Fig 6**. Ultrasound image of a hemangioma in a 17.5 millimeter by 17.5-millimeter Region of Interest (ROI) (as shown in **Fig 6**(1)). The direct reconstruction method (**Fig 6**(2)) was used to recreate the Young's modulus with respect to the liver by fixing the analytical figure of Young's modulus at the ROI frontier to unification. While the outside of the hemangioma is clearly tougher than the surrounding tissue, the inside is softer. The softer inner component of this distribution is more clearly portrayed in the model-based EI (see **Fig 6**(3)). Early attempts at MBR depicted the hemangioma as a monolithic, spherical inclusion. The error function was minimized throughout the ROI to reconstruct the comparative Young's modulus, output force, and histopathologic center (x_0, y_0) for a certain quantity of layers.
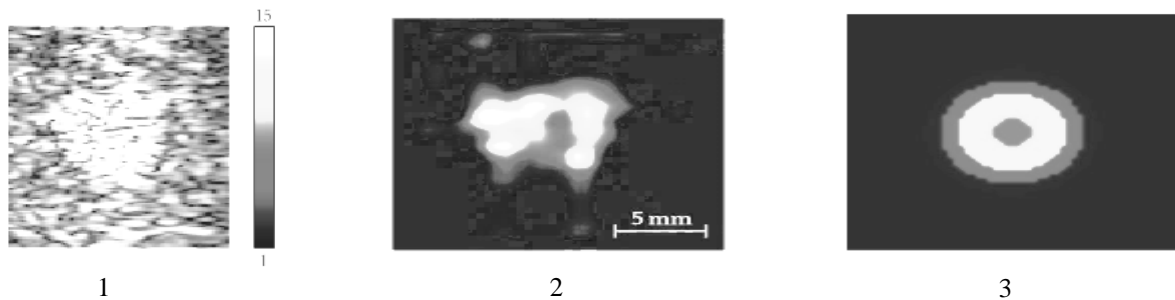

Fig 6. Hemangioma pictures acquired through B-scan (1), direct technique (2), and model-based (3) EI
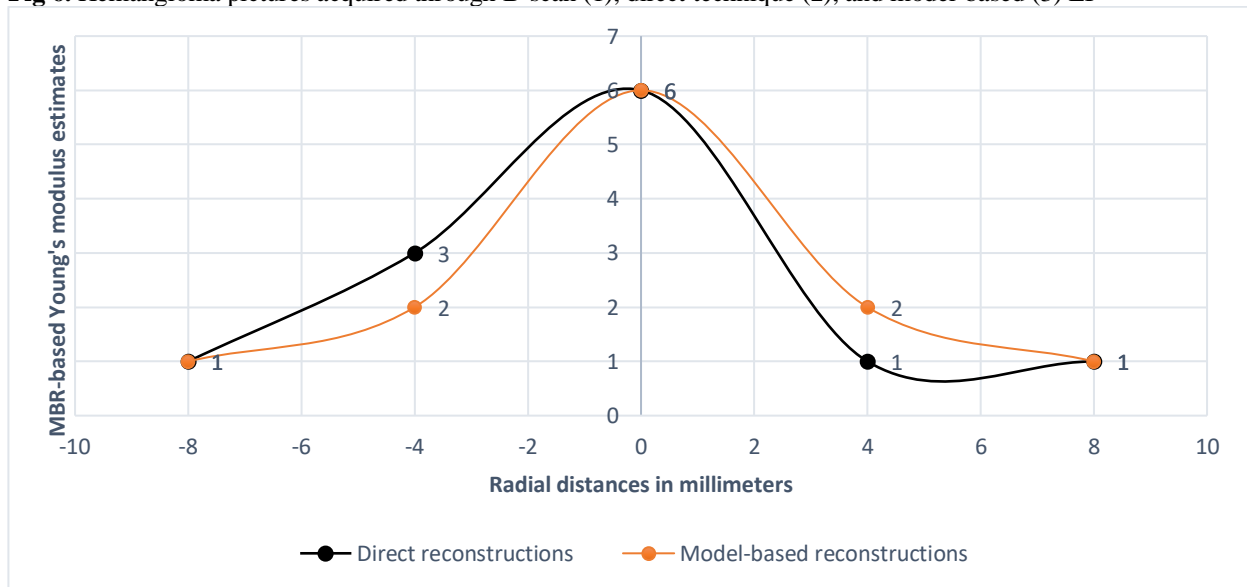

Fig 7. The empirical and MBR-derived Young's modulus estimates are examined across a continuous path at the middle of the hemangioma.

Comparison of the Young's modulus dispersion along the solid line through the hemangioma's axis (**Fig 7**) reveals a high degree of concordance between the two modeling techniques. Only 12 layers were employed to characterize hemangioma in the MBR technique. The results shown in **Fig 9, Fig 10,** and **Fig 11** agree with the expected elasticity distributions within the hemangioma, where the encapsulation surrounding the tumor makes the lesions harder than normal. The intricate make-up of these tumors may be captured using reconstruction EI. This research provides promising

evidence that reconstructive EI may be used to diagnose hepatic hemangiomas. Since all lesions may yield overall fairly similar strain pictures, strain imaging alone may not be adequate to identify hemangioma from other forms of liver cancers. The rebuilt elasticity map, on the other hand, may reveal key variations among the tumors.

ER of Deep Vein Thrombosis

Combining sonification and color coding In addition to traditional B-mode sonography, Doppler imaging is also used to make this assessment in real time (two-dimensional grayscale US). Compression ultrasonography is a scan of the patient's leg veins and arteries from a transverse angle. At regular intervals, the operator applies pressure to the patient's leg in order to lengthen the veins and arteries just under the surface. If an adjacent artery widens but a vein does not, this is indicative of a clot. Elastic imaging may be easily incorporated into the current method of DVT diagnosis, as compression ultrasound already comprises all the necessary components. (that is, changes to the shape of the object as seen from the outside during continuous ultrasounds).

Stasis-induced venous thromboembolism was simulated in rats for this study. The Institution of Michigan's Advisory board for the Utilization and Treatment of Living creatures approved the experiment only after it was undertaken in conformance with the NIH's guidelines for the treatment and utilize of research lab animals. Only four of the five rats used in the study developed thrombosis, but the findings were nonetheless noteworthy. All of the rats' Inferior Vena Cava (IVC) thrombus formation was surgically induced on day one. On the third, fifth, sixth, seventh, eighth and tenth days, scans were performed on each rat to track the development of thrombi from the acute to the chronic stages.
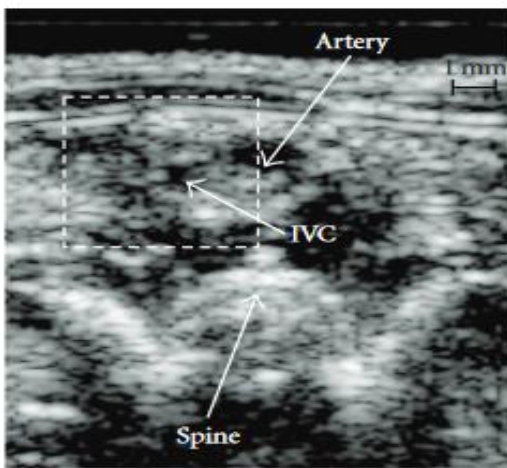
Fig 8. Abdominal B-scan ultrasonography in a rat
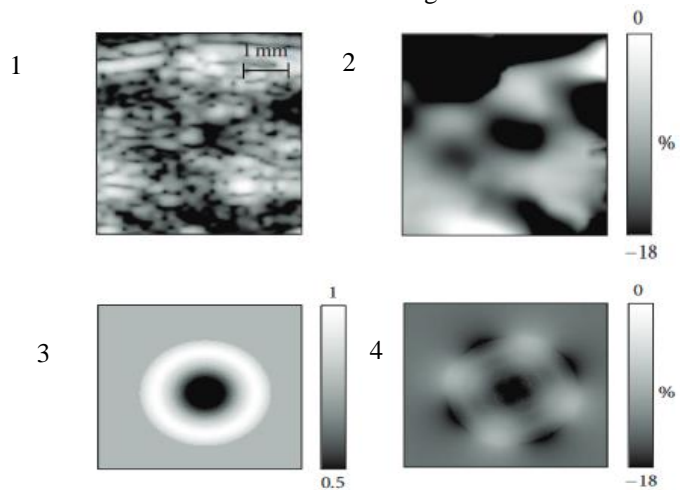
Fig 9. A rat with a thrombus that had formed 5 days earlier had a treatment to rebuild its elasticity. A 4.5-millimeter 4.5-millimeter area was chosen for elasticity rebuilding (a). As for (b), it's a picture of the axial load that was recorded within the active ROI. Variation of Young's modulus (c) as determined through reconstruction. The model parameters axial strain picture is shown in (d).

Every ultrasound was taken using a Siemens "Elegra" scanner equipped with a dimensional 12 MHz component transmitter (VFX13-5). Initial studies with both vertical and horizontal doppler configuration on the IVCs helped locate the hematoma and pinpoint the optimal probe placement on the rat's ribcage. Next, transverse stress was applied using the transducer to the tissue between the rat's lower abdomen as well as the organs below. It was secured to a manually deforming mechanism to provide a steady state of compression. Continuous phase-sensitive ultrasound frame recordings were made throughout the length of the distortion, which persisted for around 6 seconds. A 2D correlation-based process speckle tracking approach applied offline to sequential pictures was used to construct the strain image of the DVT and surrounding structures. The lateral kernel size we agreed on for cross-correlation was 0.60 mm, while the axial kernel size was 0.17 mm. A Quantization filter with 1.2 mm edges and 0.9 mm axes was used to refine the similarity function. After that, axial stress and strain were approximated mathematically by adding up deformations across consecutive images within a single flexural series.

The first step towards reconstructing the animals' elasticity was looking at their B-scans of the thrombus area (see **Fig 8**). The ultrasound image was used to pinpoint the clot's epicenter and select ROIs for elasticity repair (x, y, 0). Because changes in reference tissue deformability can have a significant impact on the results, evey ROI was specifically selected to include only the IVC and a bare minimum of interstitium (see **Fig 9**). The Young's modulus can be seen relatively using the ER tool, but absolute reconstruction calls for information on the surface stress distribution in response to external deformations. Accordingly, it was decided that a vessel wall's Young's modulus of 1 would be an appropriate starting point.

The suggested method needed some tweaking so that we could recover DVT elasticity. We assume the external load is given at an angle to the axis of the ultrasound beam. The angle was included as a parameter to the minimization formula

for further refinement. The geometry of the thrombus, the vessel, and the surrounding tissue is supposed to be that of a long, round cylinder containing the clot. It was anticipated that the clot would maintain a uniform cylindrical shape early on in the reconstruction process. The coordinates (x, y, 0) of the clot's core were determined by eye using the ultrasound image as a guide.After determining a method that was feasible up to a specific number of rings, we increased that number to ensure that a sufficient number of rings was used to describe the item. After interpolating the previous elasticity distributions and stress variables with 0, the next phase was to approximate the thrombo, circulatory system, and surrounding structures with extra dimension rings with variable elasticity. This process was repeated until there was less than a 2% difference between any two iterations of the simulation (— for example, Elastic modulus computations for varying numbers of layers). The exact number of layers in a final Young's modulus map might vary from 30 to 40, depending on the data set under consideration.

In **Fig 8**, we see a B-scan image of the abdomen of a five-day-old rat with a thrombus. The axial and lateral dimensions of this image are 10 and 8.5 millimeters, respectively. Because no blood flow was seen in the IVC itself, we were able to detect that the adjacent artery was blocked by the thrombus, thanks to color-flow imaging. On the B-bottom, you can see the spine's front. In Fig. 9, we see the outcomes of a hypothetical Elasticity Reconstruction (ER) for the exact same rat. **Fig 9**(1) displays the 4.5-millimeter 4.5-millimeter ER zone selected to contain the entire IVC, the thrombus in the center, and some surrounding tissues. Measurements of the axial strain are shown in **Fig 9**(2). Strain is shown in white and typical axial strain magnitude is shown in black throughout a strain range of 0% to 18%. (If the strain is negative, then the venous size shrank upright during the deflections).

Then, an ER method was used by recalculating the conceptually predicted longitudinal strain chart (yy theory) and comparing it to the experimentally observed dispersion of strain. In **Fig 9**(3), we see a grayscale map representing the resulting dispersion of Young's elastic modulus throughout a set of rings in the range (0.5 to 1.0). On this grayscale chart, white represents places with a comparative Moduli greater or equal to 0.5, while black represents areas with a lower modulus. Reconstructed Young's modulus values (shown in **Fig 9**(4)) are used to predict the axial strain distribution.
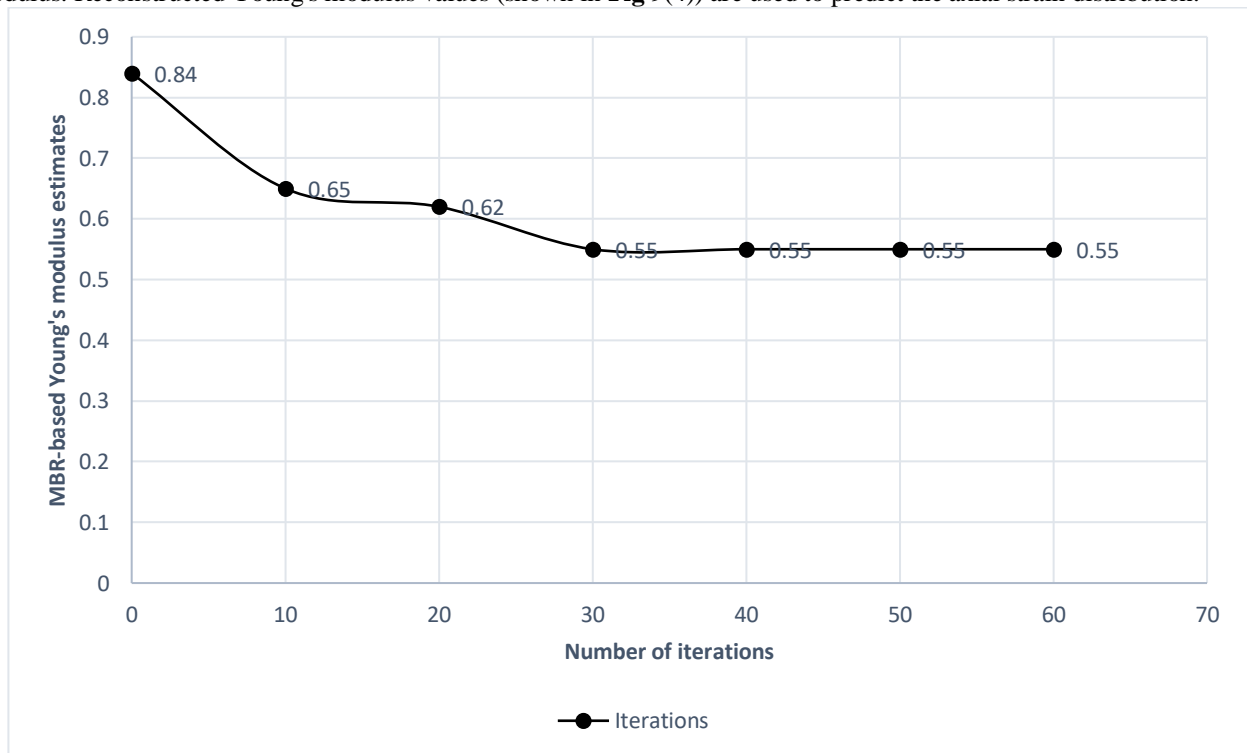
Fig 10. Blood clot approximation employing 5 rings or layers, shown against iterations to determine relative Young's modulus. Using the results of the 4-ring model, an initial value was selected for the iterative process. These findings are in line with what is shown in **Fig 8** and **Fig 9**. (5-day old thrombus in a living creature).

The information in **Fig 8** and **Fig 9** is representative of these specific findings (5-day old thrombus in a living creature) **Fig 13** gives an approximate elastic modulus pattern for thrombi from a separate animal at ages 4, 7, and 10. As the vessel constricts throughout the clotting process, the location of the vessel walls changes over time. Images depicting the reducing process may be seen in **Fig 13** and **Fig 14**. Changing Young's modulus as a function of iterations is seen in **Fig 10**. Assume that there are five levels in this example. Before, we established a base for the elasticity calculation by setting the number of layers to 4. Every iteration aimed to reduce the error function as much as possible. Convergence speeds are increased by a factor of 5-10 times when regions demonstrating fast elasticity change (at iterations 5 and 25) are correlated with strong global linear prediction. The comparative ductility of the thrombus is seen in **Fig 11** as the ring count increases. These findings show that for this experimental dataset, 30–40 rings are sufficient to accurately represent the

blood to clot, vascular wall, and underlying structures, while increasing the number of rings seemed to have no influence on the outcome.
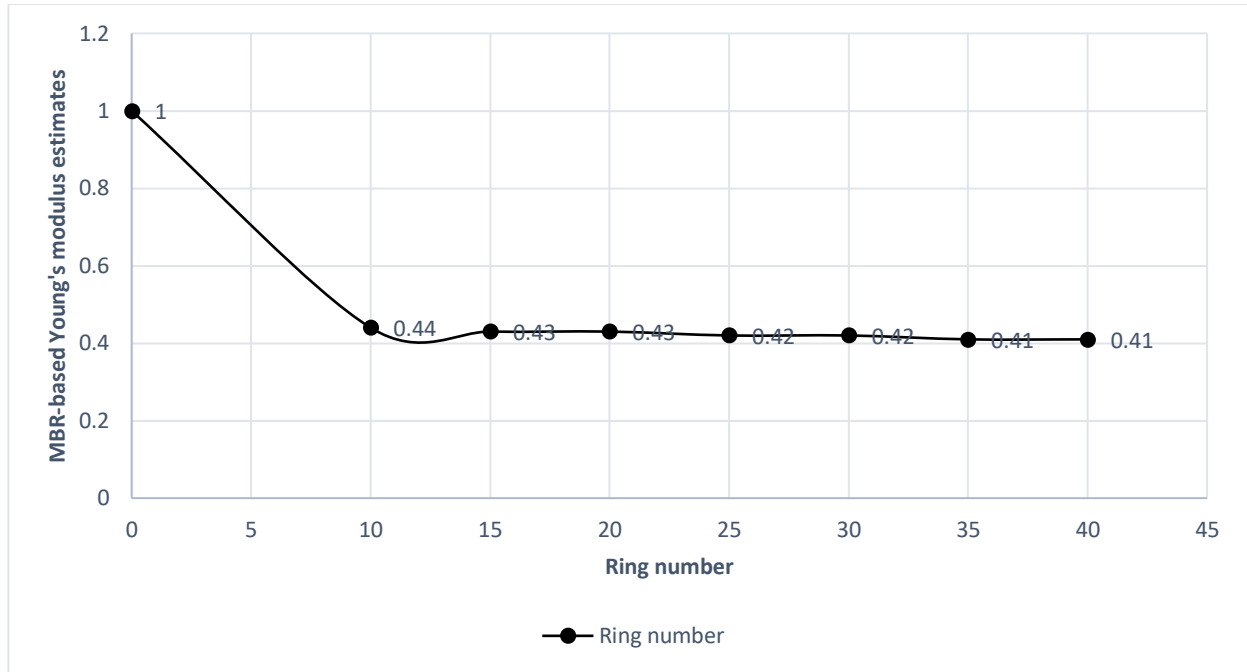

Fig 11. A visual depiction of how the Young's modulus varies with the thickness of an object's layers or rings.

Fig 12 presents a comparison of the Young's modulus accounts at the thrombosis's center for one of the animals at five, eight, and ten days postoperatively (findings seen in in Fig. 8 to Fig. 11 are consistent with the general trend for thrombosis older than 5 days).
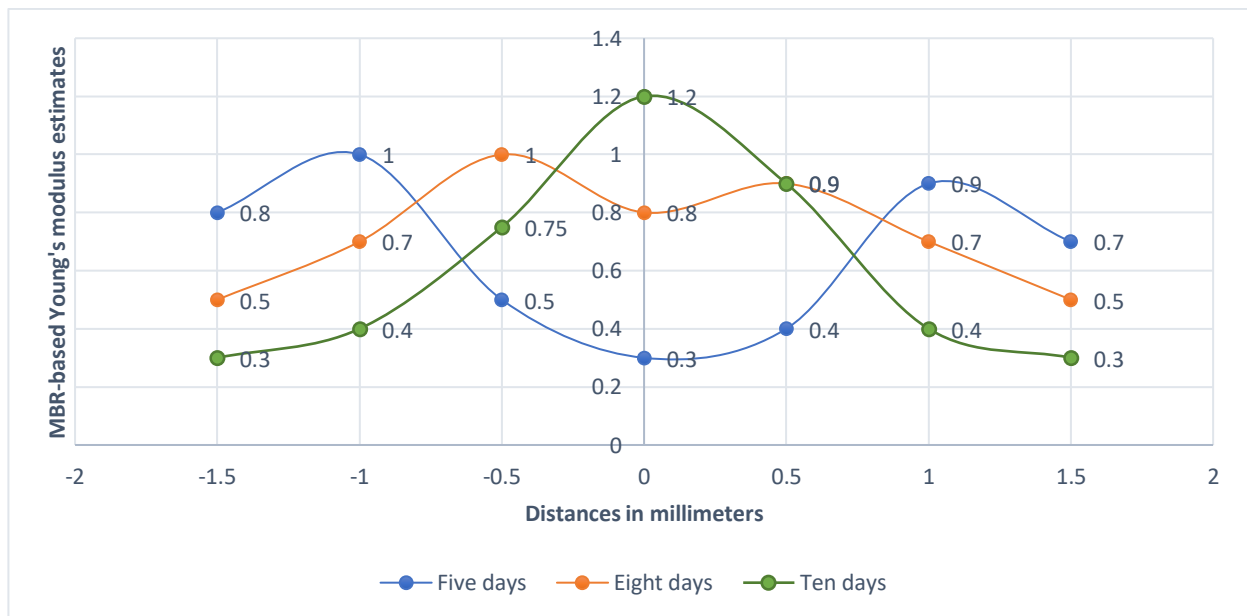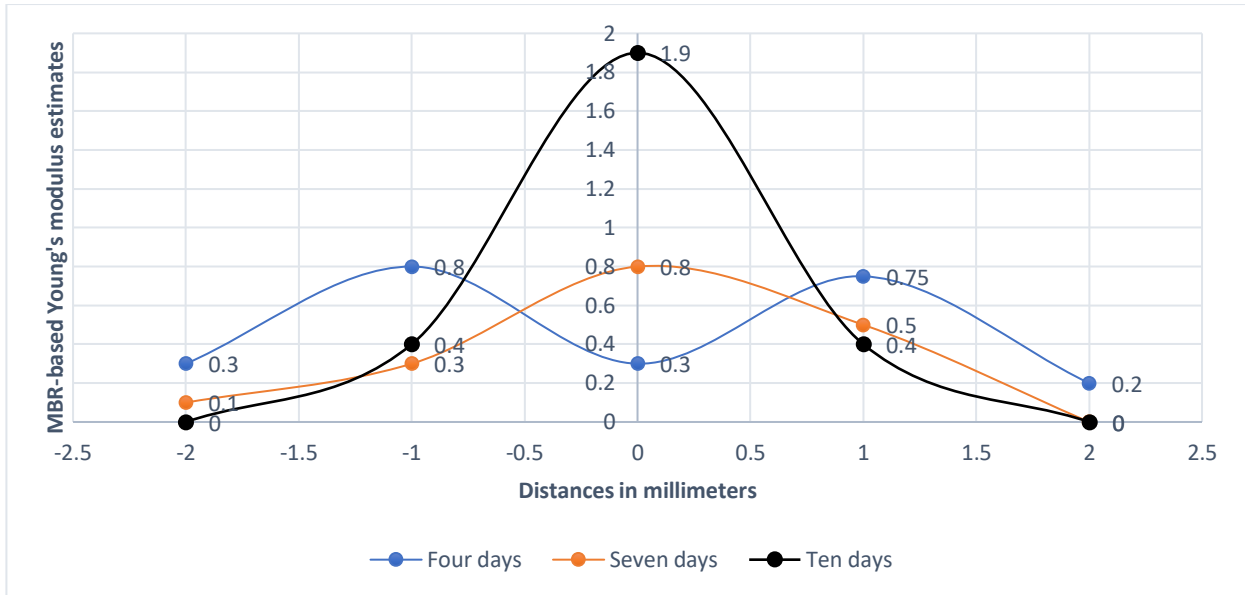

Fig 12. Comparison of acute (eight days), subacute (eight days), and chronic (ten days) thrombus Young's modulus patterns

Fig 13. Assessment of Young's modulus patterns for thrombi that are four days old (acute), seven days old (subclinical), and ten days old (cyclic).

Acute DVT is represented by thrombus between three and four days old in this animal model, subacute DVT by thrombus between six and seven days old, and chronic DVT by thrombus more than ten days old. Although the growing rate of thrombi in humans varies, the steps involved in clot formation are universal. The flexibility of the thrombus improves as it grows. **Fig. 14** further illustrates this concept by showing a graph of relative Young's modulus vs thrombus age.
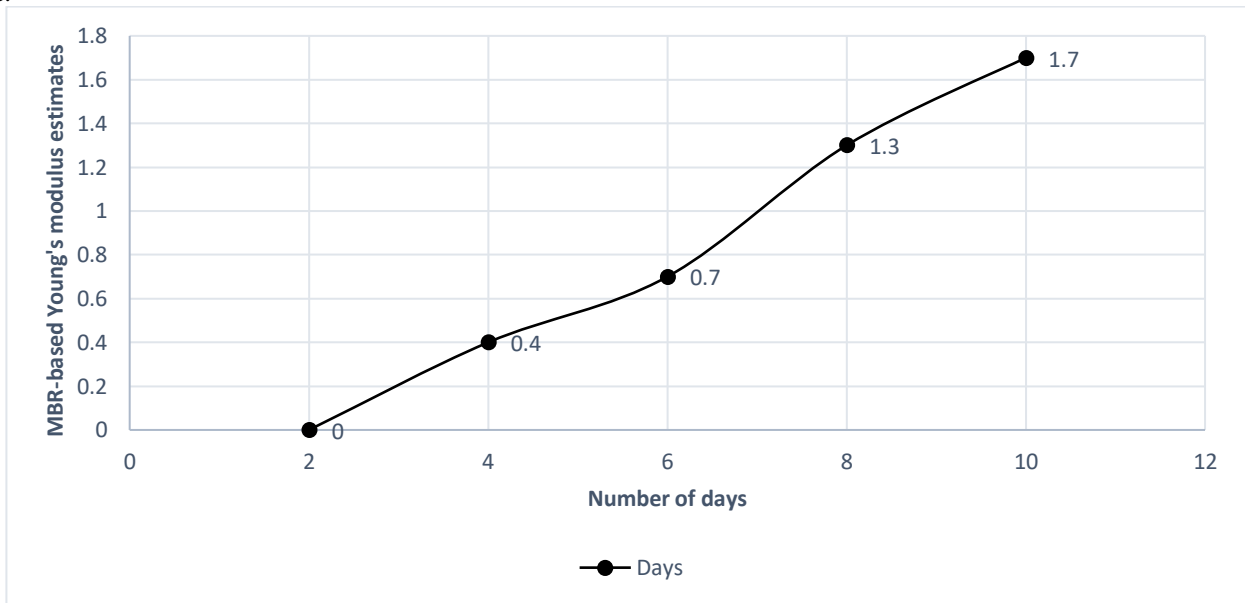

Fig 14. Thrombus relative Young's modulus parameters rebuilt using a model of thrombus development and aging.

A mean elasticity score was determined for the 4 rats used in this study. Since the thrombus's relative elasticity increases with age, Elastic modulus might be used to estimate the age of a DVT. Ex vivo direct elasticity assessments were compared with in vivo ERs findings. Fifty-nine Sprague-Dawley rats were used for the research. The set of animals (nine to thirteen in total) were killed on days three, six, ten, and fourteen so that parameters of Young's modulus of the clots could be taken. After the IVC was cut, the thrombi were extracted and sent to the next room to be subjected to mechanical load-displacement tests in order to determine the thrombi's Young's modulus with precision. For this study, we examined the compression-induced displacement as a function of applied force. The strain-stress relationship and finite element modeling of the clot distortion were used to determine the experimental specimen's Moduli.

The first tests of the device were performed on a cylinder of rubber with known elastic characteristics. The elasticity was tested directly in vivo, and the results were recorded utilizing a strain range of 15 percent to 20 percent. Ultrasound in vivo research often use strain levels in this range. Young's modulus was measured mechanically ex vivo and the results are

presented as a measure of thrombo age in **Fig 15**. The in vivo reconstructions are in good agreement with the ex vivo dynamic data, as shown in **Fig 14**, and **Fig 15**. Both in-person and indirect measurements of clot rigidity show that a thrombus solidifies with time. Actually, thrombi become tougher as time goes on; a thrombus that has been around for ten days has a Young's modulus that is three to six times that of a thrombus that has just been there for three days. Therefore, a DVT animal model may benefit from the model-based ER strategy. Probabilistic model-based restorative EI may be used to properly measure and monitor the increasing elasticity of the thrombus over time.
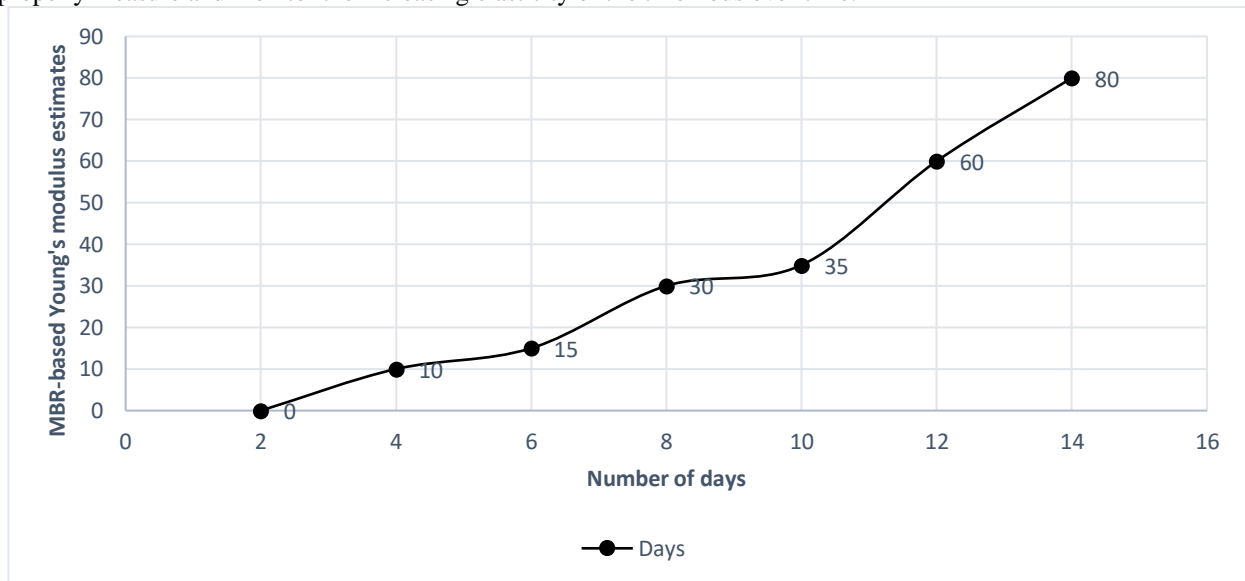
Fig 15. The Young's modulus of the thrombus directly measured mechanically ex vivo throughout thrombus development and aging.

V. CONCLUSION

Elasticity Imaging (EI) is a relatively new type of imaging that allows researchers to visualize elastic tissue parameters associated with the structural operation of both healthy and diseased tissues. In this article, we presented two potential therapeutic applications of the model-based Elasticity Imaging (EI) approach: the detection of liver hemangiomas and the distinction between Deep Venous Thromboses (DVT). To obtain the expected results, Liver hemangiomas were supposed to have spherical symmetry, while DVT was thought to have a cylindrical shape. Both investigations employed external surface deflections during continuous ultrasound scanning, with tissue mobility evaluated using a block-matching cross-correlation technique. The Young's modulus was computed using strain images. Elasticity Reconstruction (ER) is a model-based method developed to validate the utility of US reconstructive EI. When compared to existing methods for ER, the model-based technique that was created provides a number of benefits. Only the axial part of the strain tensor is needed for the model-based ER. The reductive strategy used in Model-Based Reconstruction (MBR) is efficient and dependable since there are only a small number of uncertain vector variables after an analytic treatment of the forward elasticity problem. Last but not least, MBR is not too picky about the specifics of external loading. Liver hemangioma and Deep Venous Thrombi (DVT) aging were both studied using model-based reconstructive EI. Our research shows that ultrasonic in vivo EI may benefit from the MBR method by providing valuable insight into tissue biomechanical features.

Data Availability
No data was used to support this study.

Conflicts of Interests
The author(s) declare(s) that they have no conflicts of interest.

Funding
No funding was received to assist with the preparation of this manuscript.

Ethics Approval and Consent to Participate
Not applicable.

Competing Interests
There are no competing interests.

References

[1]. D. C. Morris, D. Y. Chan, M. L. Palmeri, T. J. Polascik, W.-C. Foo, and K. R. Nightingale, "Prostate cancer detection using 3-D shear wave elasticity imaging," Ultrasound Med. Biol., vol. 47, no. 7, pp. 1670–1680, 2021.

[2]. H. Xiang, W. Ling, L. Ma, L. Yang, T. Lin, and Y. Luo, "Shear wave elastography using sound touch elastography and supersonic shear imaging for liver measurements: a comparative study," Quant. Imaging Med. Surg., vol. 12, no. 5, pp. 2855–2865, 2022.

[3]. S. Yuan, H. Shao, Z. Na, M. Kong, and W. Cheng, "Value of shear wave elasticity in predicting the efficacy of neoadjuvant chemotherapy in different molecular types," Clin. Imaging, vol. 89, pp. 97–103, 2022.

[4]. S. A. McAleavey, "Shear modulus imaging by Spatially Modulated Ultrasound Radiation Force," in 2009 IEEE International Ultrasonics Symposium, 2009.

[5]. L. Zhao, H. Lin, Y. Hu, X. Chen, S. Chen, and X. Zhang, "Corneal Lamb wave imaging for quantitative assessment of collagen cross-linking treatment based on comb-push ultrasound shear elastography," Ultrasonics, vol. 116, no. 106478, p. 106478, 2021.

[6]. H. Chen et al., "Detection and imaging of prostate cancer using acoustic radiation force impulse imaging and quantitative ultrasound," J. Acoust. Soc. Am., vol. 145, no. 3, pp. 1859–1860, 2019.

[7]. R. Kishimoto et al., "Shear wave speed measurement bias in a viscoelastic phantom across six ultrasound elastography systems: a comparative study with transient elastography and magnetic resonance elastography," J. Med. Ultrason. (2001), vol. 49, no. 2, pp. 143–152, 2022.

[8]. V. Gapyak, T. März, and A. Weinmann, "Quality-enhancing techniques for model-based reconstruction in magnetic Particle Imaging," Mathematics, vol. 10, no. 18, p. 3278, 2022.

[9]. C. E. Miller, J. H. Jordan, A. Thomas, and J. A. Weis, "Developing a biomechanical model-based elasticity imaging method for assessing hormone receptor positive breast cancer treatment-related myocardial stiffness changes," J. Med. Imaging (Bellingham), vol. 8, no. 5, p. 056002, 2021.

[10]. N. Nitta, T. Shiina, and E. Ueno, "Tissue elasticity reconstruction based on three-dimensional displacement data estimated by the weighted phase gradient method," in 1999 IEEE Ultrasonics Symposium. Proceedings. International Symposium (Cat. No.99CH37027), 2003.

[11]. M. M. Gubenko et al., "Video-tactile pneumatic sensor for soft tissue elastic modulus estimation," Biomed. Eng. Online, vol. 16, no. 1, 2017.

[12]. B. Damascelli et al., "Combined modes of imaging for liver hemangioma in cancer patients," Tumori, vol. 68, no. 6, pp. 485–497, 1982.

[13]. S. Metikala et al., "Integration of vascular progenitors into functional blood vessels represents a distinct mechanism of vascular growth," Dev. Cell, vol. 57, no. 6, pp. 767-782.e6, 2022.

[14]. S. Adjei et al., "Mortality risk among patients hospitalized primarily for COVID-19 during the Omicron and Delta variant pandemic periods - United States, April 2020-June 2022," MMWR Morb. Mortal. Wkly. Rep., vol. 71, no. 37, pp. 1182–1189, 2022.

[15]. H. V. Joffe, N. Kucher, V. F. Tapson, S. Z. Goldhaber, and Deep Vein Thrombosis (DVT) FREE Steering Committee, "Upper-extremity deep vein thrombosis: a prospective registry of 592 patients," Circulation, vol. 110, no. 12, pp. 1605–1611, 2004.

[16]. Y. Liu et al., "The added value of vessel wall MRI in the detection of intraluminal thrombus in patients suspected of craniocervical artery dissection," Aging Dis., vol. 12, no. 8, pp. 2140–2150, 2021.

[17]. D. P. Krowchuk et al., "Clinical practice guideline for the management of infantile hemangiomas," Pediatrics, vol. 143, no. 1, p. e20183475, 2019.